Research Summary

The Thermal Spray Processing of HA Powders and Coatings

K.A. Khor, P. Cheang, and Y. Wang

In recent years, coated implants have been actively researched and put to use in many biomedical engineering applications. The coating used on the implants is hydroxyapatite (HA), a calcium-phosphate compound with attractive bioactive and biocompatible properties that can enhance the fixation process of biomedical implants. Thermal spraying provides a potent means for depositing the HA coatings on implants. Among the popular thermal-spray techniques are combustion-flame spray, plasma spray, and high-velocity oxy-fuel spray. This article investigates the versatility of thermal-spray techniques to perform spheroidization of HA powders, the preparation of HA-based biocomposite powders and coatings, and the deposition of HA coatings.

INTRODUCTION

Hydroxyapatite (HA) is a bioactive material with a calcium-to-phosphorus ratio that is similar to that of natural bone, and this can encourage early bonding between bony tissues and the implant surface.[1,2] The provision of a high-calcium and phosphorus-rich environment promotes rapid bone formation within the vicinity of the implant; studies have shown bone growth into the open pores on the surface of HA implants in both animal tests and human bodies.[3–6] Variable amounts of new bone formation, along with mature fibrous tissues, were also found surrounding the implants.[7]

Dense HA can be formed by hot pressing or normal pressure sintering.[8] However, there are concerns with regards to the wide variation in sintering behavior and the resultant mechanical properties of sintered HA; a recent study shows that sintering characteristics are influenced by raw-powder morphology.[9] One serious drawback to the application of dense, sintered HA is the development of cracks in load-bearing implants,[10] which has severely curtailed the usage of HA.

An alternative to the application of HA in the human body is as a coating on bioinert metallic implants.[11,12] Among the many biological advantages of the HA coatings are the enhancement of bone formation, accelerated bonding between the implant surface and surrounding tissues, and the reduction of potentially harmful metallic ion releases.[13–16] HA has been applied as a coating on many types of implants such as hip and dental applications.[17,18] HA also establishes strong interfacial bonds with titanium implants;[19] this is apparently attributed to some chemical bonding between HA and the titanium substrate.[20]

HA coatings have been applied on various substrates by a wide range of surface deposition techniques such as plasma spraying, high-velocity oxy-fuel (HVOF) spraying, ion-beam sputtering, pulsed laser ablation, electrophoretic deposition, radion frequency (r.f.) magnetron sputtering, and sol-gel and conventional ceramic processes that involve pressing and sintering.[21–29] Among these surfacing processes, thermal-spray techniques offer the attractive prospect of economy and efficient deposition of HA. Additional background on thermal-spray techniques and HA composites can be found in the sidebar.

This article reports the results of a study on the use of thermal-spray techniques to process HA powders and deposit HA coatings for biomedical implants. Spheroidized HA and HA-based composite powders produced by combustion-flame spray were used as feedstock for the plasma spray and HVOF spray processes to form the HA coatings on the substrates.

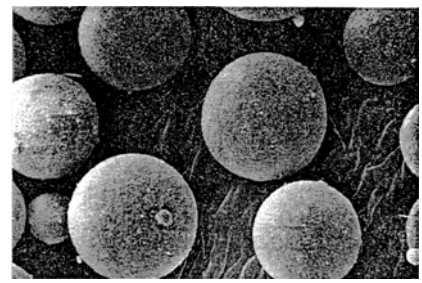

20 μm

Figure 1. An SEM of flame-spheroidized HA powders.

EXPERIMENTAL PROCEDURES

HA powders were prepared by reacting orthophosphoric acid with calcium hydroxide at specific mole concentrations. The gelatinous precipitate was separated and dried in an oven at 180°C for more than 24 hours. The hardened cake was subsequently crushed and sieved to various sizes suitable for thermal spraying. X-ray diffraction (XRD) analysis indicated that the as-prepared HA powders were predominantly pure HA.

Heat treatment at 800°C for two hours significantly increased the crystallinity of the as-prepared HA powder. This was probably due to the growth of the fine crystallites in the agglomerated particles and the transformation of some amorphous phases to crystalline HA. Two batches of calcined HA (CHA) powders (75–106 μm and 56–75 μm) were sieved and used in the preparation of the HA coatings. Although pure and crystalline HA feedstock was used, thermal spraying of this powder did not produce coatings with the same degree of purity and crystallinity as found in the starting material.

The thermal-spray techniques used were plasma spray, combustion-flame spray, and HVOF spray. Combustion-flame spraying was performed with the Miller FP 73 flame torch, using a mixture of oxygen and acetylene gases. The role of combustion-flame spray was primarily powder spheroidization. CHA powders were flame-sprayed into distilled water in a stainless steel container and sieved into the following size ranges: 125–175 μm, 45–75 μm, 20–45 μm, and 5–20 μm. The flame-spheroidized powders were subsequently sprayed by plasma spray and HVOF spray to form HA coatings on prepared substrates. A 40 kW plasma spray (SG-100, Miller Thermal) was used to deposit the spheroidized HA feedstock. Argon was the main plasma-forming gas, and helium was the auxiliary gas. Table 1 lists the plasma-spray parameters. The powder feed was assisted by a computerized, closed-loop, rotor-feed hopper. The HVOF system used was the HV 2,000 (Miller Thermal), which can operate using propylene, acetylene, propane, and hydrogen as the fuel gas. It consists of a gas-control unit, powder feeder, gun-cooling system, and spray gun. The HVOF flame was formed by the combustion of oxygen and hydrogen.

Table 1. Plasma Spray Parameters for the Deposition of Ti-6Al-4V/HA Coatings

Primary Gas	Argon (344.75 kPa)
Auxiliary Gas	Helium (344.75 kPa)
Anode	Forward Feed
Cathode	Subsonic
Powder Feed Rate	3.5 rpm
Stand-Off Distance	12–14 cm

Scanning electron microscopy (SEM) was performed with the Cambridge Stereo Scan S360 equipped with an energy-dispersive x-ray analyzer (EDX). Phase analysis of the spheroidized HA powders and thermal-sprayed HA coatings was performed on the Philips MPD 1880 x-ray diffractometer system. Particle size distribution measurements were made using the x-ray sedimentation technique (Sedigraph 5100, Micromeritics) and laser-diffraction technique (Fritsch Analysette 22, Germany).

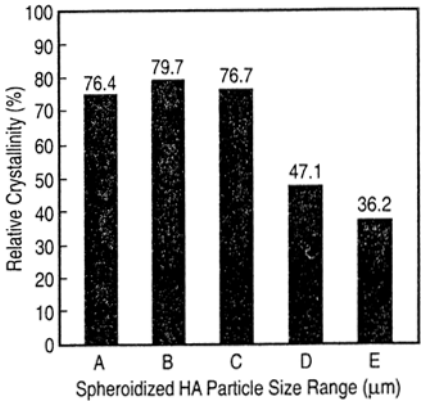

Figure 2. The relation of relative crystallinity (C_r) of flame-spheroidized HA powders with respect to different size ranges. (A—all sizes, B—75–125 μm, C—45–75 μm, D—20–45 μm, E—5–20 μm).

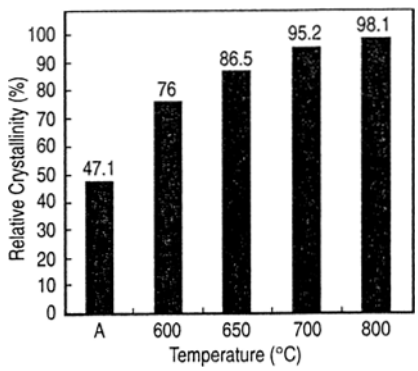

Figure 3. The progressive increase in C_r of flame-spheroidized HA powders following heat treatment.

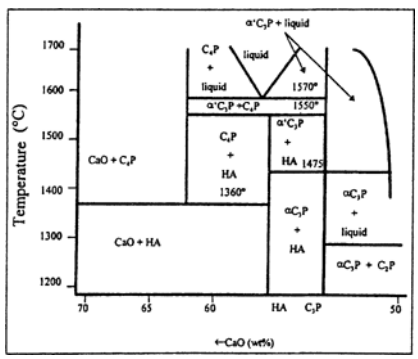

Figure 4. The binary phase diagram of the $CaO-P_2O_5$ system.

COMBUSTION-FLAME SPHEROIDIZATION OF HA POWDERS

SEM observation of the flame-spheroidized HA powders (see the "Experimental Procedures" sidebar) indicates that spheroidization converts all of the porous, agglomerated, angular CHA particles to highly dense and spherical particles (Figure 1). Virtually all of the particles below 80 μm have been effectively spheroidized. This confirmed the limit of the combustion-flame spray process in the melting of HA. Although some CHA particles are initially spheroidized using a plasma-spray technique, the resulting powders show a wide particle size distribution. This may be due to particle breakdown of the weak CHA in the turbulent plasma jet. In addition, XRD showed the plasma-spheroidized HA possessed an undesirable high content of amorphous calcium phosphate phases, while the flame-spheroidized HA was composed of highly crystalline HA.

The amorphorization of the HA appears to be most significant in the fine HA powders (<45 μm). Compared to the combustion flame, the plasma flame is hotter (>10,000°C) and the heating rate is extremely high, but the melting zone is relatively small. Also, the treatment of the particles may not be uniform because of nonaxial feeding of the powders.

Both plasma- and combustion-flame spheroidized HA have a spherical geometry, dense internal structure, and a smooth, glassy surface. XRD analysis of the flame-spheroidized HA shows high crystalline content; there is relatively little loss in the amount in crystalline HA phase when compared with plasma-sprayed HA powders. However, the relative crystallinity, C_r, becomes progressively lower with decreasing particle size (Figure 2). This is consistent with the formation of amorphous calcium-phosphate phases when the powders are rapidly quenched. The smaller particle-size ranges would likely be completely molten at the point of impact on the distilled water surface compared with larger particles (>75 μm) where, perhaps, the outer surface may be completely molten, but the inner core of the particles may not have melted. However, EDX analyses show the Ca/P ratio to be more uniform in the different size fractions (75–125 μm, 45–75 μm, 20–45 μm, and 5–20 μm) of flame-spheroidized HA.[70–72] This could likely be due to the lower incidence of particle dissociation in the lower-temperature combustion flame. The crystallinity of the particles in the lower particle-size ranges can be increased through further heat treatment at 600–800°C prior to plasma spraying. Figure 3 shows the progressive increase in C_r with respect to the heat-treatment temperature employed. A significant increase in C_r was observed from 600–700°C.

Coatings generated from spheroidized powders have unique surface and microstructure characteristics. The binary phase diagram of $CaO–P_2O_5$ indicates that any deviation in the chemical composition of HA during solidification would result in the formation of other calcium-phosphate phases (Figure 4).[73] XRD analysis of plasma-sprayed particles as a function of particle size is shown in Figure 5. It can be observed that the CaO phase (major peak at $2\theta = 38.0°$) starts to appear in the smaller size range of 10–20 μm. The particle morphology/geometry as a function of particle size is summarized in Table I.

PLASMA-SPRAYED HA POWDERS

Plasma-sprayed HA coatings are known to contain other bioresorbable phases such as tricalcium phosphate (TCP), tetracalcium phosphate (TTCP), calcium oxide (CaO), and amorphous calcium phosphate (ACP). In order to ascertain the occurrence of these transitional phases and the structural amorphicity of as-sprayed coatings, the chemical, physical, and structural conditions of the in-flight particles require better understanding. Hence, the physicochemical states of the thermally sprayed particles were preserved as they emerged from the plasma flame by quenching into water. CHA particles were used as the feedstock. Plasma-spheroidization studies indicate that the physicochemical condition of as-sprayed particles is a strong function of the starting particle size, stability, and thermal treatment. Large particles above a certain size remained unmelted with little or no change in shape and structure, while smaller particles experienced substantial physical, chemical, and structural changes.

Weak, agglomerated particles that were poorly bonded experienced significant particle fragmentation during passage through the turbulent plasma, resulting in the formation of smaller particle sizes. These smaller particles subsequently attained different temperatures and transitional states, depending on their relative size and degrees of thermal treatment. As a result, the plasma-particle interaction (and, hence, physicochemical transformation) was expected to differ among particles of different sizes. Consequently, the final coating microstructure significantly depends on the resultant phase and structural characteristic associated with the fragmented particle-size distribution.

As verified by XRD analysis, larger particles above 75 μm were crystalline HA and angular in shape, showing little or no melting. This suggests that particle sizes above 75 μm may be unsuitable for plasma spraying because of the tendency to form a porous microstructure comprising partially melted particles with a high degree of crystallin-

ity. Sprayed particles ranging from 30–55 μm had mixtures of crystalline and amorphous phases, but the shape of the particles was generally spherical or oval. Sprayed particles of less than 30 μm were predominantly spherical and contained large amount of amorphous phases. CaO was detected in the size range of 10–20 μm. In addition, preliminary Fourier transform infrared spectroscopy (FTIR) work revealed the molecular bonding between species, as reflected by characteristic frequency or wavelength.[71] This technique was sufficiently sensitive to detect minute changes and deviation in the spectral profile associated with the physicochemical transformation as a function of particle size. Hence, this particle-plasma interaction suggests that particle size and stability during deposition is an important factor (in terms of the phase, crystallinity, and microstructure) in the final characteristic of the coating.

A schematic diagram summarizing the effect of particle size on the physical state, phase content, and geometry of sprayed HA particles (melted/semimolten/unmelted) as a result of plasma-particle interaction is shown in Figure 6. From the diagram, large particles above S_m do not melt at all. These are likely to bounce off or become lodged in the coating, thus, generating considerable porosity. Particles between S_m and S_s experience partial melting. The maximum spheroidization diameter, S_c, lies within this range. Between S_m and S_s, the outer surface of the particle has a smooth glassy appearance with the inner body having the same agglomerated structure as the starting powder. Particle sizes less than S_s are completely molten, forming a spherical droplet geometry prior to hitting the substrate.

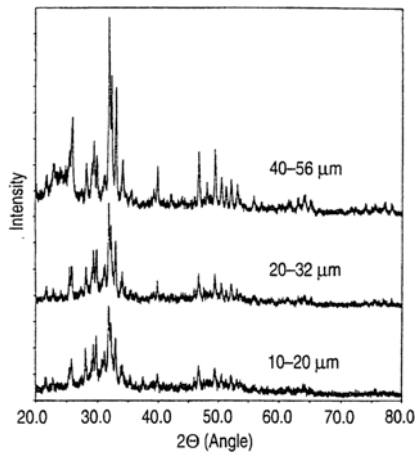

Figure 5. An XRD analysis of plasma-sprayed particles as a function of particle size.

PLASMA SPRAY AND HVOF DEPOSITION

Coatings generated from two batches of CHA powders (75–106 μm and 56–75 μm) contained ACP, CaO, and small traces of TCP in addition to crystalline HA. The formation of amorphous and metastable phases is not uncommon, particularly with nonequilibrium processes like thermal spraying; however, the consequences are more severe and less tolerable in biomedical applications, where such additional phases can induce unfavorable tissue responses. Heat treatment of the coatings at 600°C, 700°C, and 800°C for one hour helped to convert the ACP and some TCP back to crystalline HA (Figure 7).

In addition to the phase content of the coating, mechanical properties are equally important because these ensure that the coating remains in place during service. Unfortunately, conditions that bring about the desired crystalline HA phases are not conducive to generating good mechanical properties because both adhesive and cohesive characteristics are associated with good melting by forming well-flattened splats that give maximum surface contact between substrate and adjoining layers. On the other hand, microstructurally dense and mechanically adherent coatings are generally amorphous, although the crystallinity can be restored with appropriate heat treatments. The presence of crystalline HA in a coating suggests a limited melting of HA, which tends to generate a porous and mechanically weak coating. This reinforces the importance of adequate melting in order to achieve a coherent microstructure with good structural strength and integrity. Coatings with an inherently poor microstructure comprising unmelted particles, pores, and irregular splat build-up generally have poor mechanical properties. Good interlamellar contact is an essential factor in

BACKGROUND

Thermal-Spray Techniques

Previous investigations have cited important relationships between thermal-spray powder morphology and coating characteristics.[30–33] HA coatings prepared by plasma spraying have been found to exhibit undesirable phenomena such as the formation of amorphous calcium phosphate, calcium triphosphate, and tetracalcium phosphate with concomitant reduction of the crystalline HA phase, deviation of the Ca/P stoichiometry, residual stresses, and the occurrence of dehydroxylation.[34–39] These detrimental consequences will reduce the potency of the HA coatings on the implants. However, such adverse effects can be significantly reduced through proper process settings and the use of raw material with appropriate characteristics. For instance, the plasma spraying of an earlier work used a wide particle size range.[40] This resulted in varying crystallinity of the coatings. In addition, the characteristics and properties of the coatings varied when the plasma-spray process was performed with different plasma-forming gases such as argon gas alone, Ar/He, or Ar/H_2. The use of inert-gas combinations that are thermally low in enthalpy showed relatively low interfacial strength and poor density, but the HA does not undergo drastic decomposition. On the other hand, the use of Ar/H_2 plasma caused significant decomposition but enhanced interfacial strength.[35,41,42] A recent study showed the contrasting results in the amount of crystalline HA phase and the amount of impurity phases when different plasma-forming gases are used.[43] Another study showed that water-loss during plasma spraying results in the formation of an OH-depleted HA. At high plasma power, P_2O_5 is lost, and the coatings contain increased amounts of CaO and $Ca_4P_2O_9$.[44]

HA-Based Composites

The limitations in HA such as brittleness, low strength, and low fracture toughness need to be addressed. As requirements in biomedical engineering applications become increasingly demanding, biomedical engineers have to consider the use of composites; however, the concept of biomedical composites is not new.[45,46]

Combining metals and polymers with HA to form bulk composites has been considered.[47] Recently, titanium and Ti-6Al-4V were combined with HA to form either bulk composites or composite coatings.[48–50] Titanium alloys have been widely utilized as biomedical implants and prosthesis because of their low density, bioinertness, and attractive mechanical properties. The addition of HA to this material would yield a composite that has both bioactive properties and good mechanical strength. Ceramics, too, have certain potentials in biomedical applications, in particular, as bioactive glasses.[51,52] Other ceramics such as alumina, titanium nitride, and transformation-toughened zirconia, although not having the kind of bioactive responses as bioactive glasses, have been shown to be biocompatible. No cytotoxicity effects were observed in tests undertaken on human differentiated cells.[53] Partially stabilized zirconia (PSZ) has featured prominently among the new class of advanced ceramics because of its superior fracture toughness and bending strength.[54–56] Yttria-stabilized PSZ has bending strength between 900–1,200 MPa and fracture toughness of 9–12.3 $MNm^{-3/2}$.[57,58] PSZ has been known to improve the fracture toughness and strength of many engineering ceramic matrices such as alumina and mullite.[59,60] In addition, it has favorable biocompatibility, showing no adverse tissue response after 3–6 month implantation.[61,62] Several studies in recent years have investigated the processing and properties of HA-ceramics composites.[63–66] Generally, the aim is to enhance the physical properties of HA with these advanced ceramics. Some investigations on PSZ-particulate-reinforced HA have also been performed.[67–69]

Table I. Particle Shape, Surface Morphology, and Phase Relative to Size in HA Powders

Size (μm)	Shape	Surface Morphology	Phases
>75	A	Porous	HA (C)
56–75	A	Smooth Outer/Porous Inner	HA (C)
40–56	S	Smooth	HA (C and Am), TCP
32–40	S	Smooth	HA (C and Am), TCP
20–32	S	Smooth	HA (A), TCP
10–20	S	Smooth	HA (Am), TCP, CaO

S—Spherical; A—Angular; C—Crystalline; Am—Amorphous.

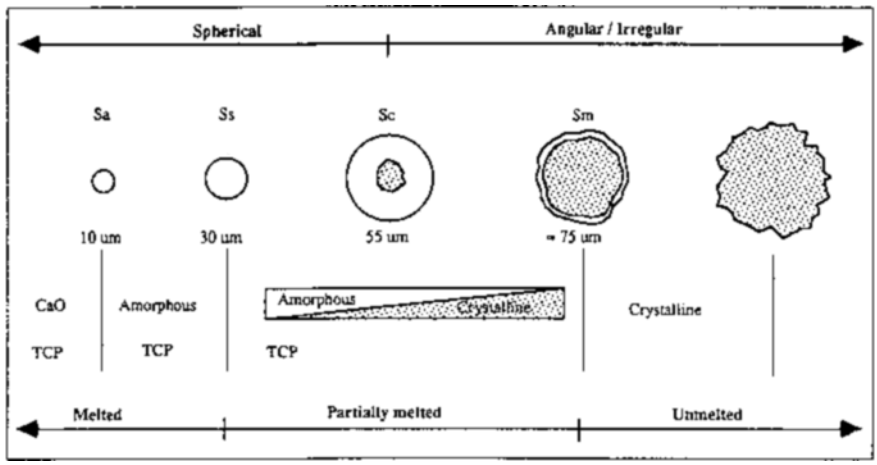

Figure 6. A schematic summarizing the effect of particle size on the physical state, phase content, and geometry of sprayed HA particles (melted/semimolten/unmelted) as a result of plasma-particle interaction.

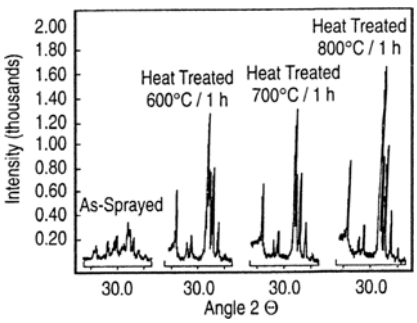

Figure 7. XRD patterns of as-sprayed and heat-treated HA coatings.

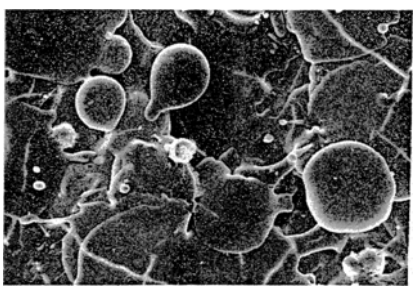

a 50 μm

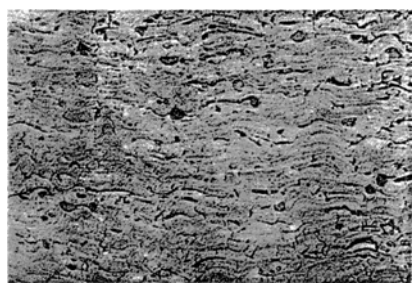

b 50 μm

Figure 8. (a) The as-sprayed surface of plasma-sprayed SHA coating and (b) the cross section of plasma-sprayed SHA coating.

Table II. Tensile Adhesion Test Data of Plasma-Sprayed CHA Coatings on Titanium

Test Number	Coating Thickness (μm)	Tensile Stress (MPa)	Fracture Mode
TC1	130	23.11	Mixed
TC2	140	26.58	Mixed
TC3	170	20.60	Mixed
TC4	170	15.26	Mixed
TC5	185	27.22	Mixed
Mean	159	22.55	

attaining high structural coherency.

From a biological-fixation viewpoint, porosity is desirable because of the possibility of tissue ingrowth into the porous structure, however, this has adverse weakening effects on the mechanical property of the coating. The pores generated during thermal spraying are normally bimodal in nature, with large pores around 30–50 μm and small pores less than 1 μm. These pore-size ranges are too small for ingrowth of soft/vascular tissue to occur.

The different phases and crystallinity of the coating will certainly exact different biological responses. Crystalline HA is bioactive in nature and is the desired phase; however, ACP is highly resorbable and will dissolve faster than the ingrowth of new bone to affect fixation. TCP, on the other hand, is considered more resorbable than crystalline HA and may, at some instances, revert to HA during implant; thus, it is acceptable in small amounts.

It must be recognized that complex interactions taking place during thermal spraying can easily result in a multifaceted microstructure with less than optimal properties. Hence, appropriate measures must be taken to ensure that the correct parameters are used to minimize this effect. These results suggest that coating consistency and quality can be compromised if certain parameters such as the coherency of starting powder (dense or agglomerate) and particle sizes are not carefully considered.

HA COATING CHARACTERISTICS

Coatings generated from spheroidized powders have unique surface and microstructure characteristics. An SEM micrograph of a coating surface reveals well-formed splats that spread and flatten to a disc configuration without disintegration (Figure 8a). This reflects adequate melting of the HA in the plasma and subsequent deposition consistency. The surface topography is generally flat with a good overlapping of subsequent spreading droplets. Porosity in the form of macropores is substantially reduced and can be further improved using a narrow particle-size distribution. This is evident from the as-sprayed coating structure of spheroidized HA (SHA) (20–45 μm, pure HA). Some microcracks are noticeable that are attributed to expansion- or contraction-stressing of the dense matrix. The cross section microstructure reveals a highly dense coating composed of randomly stacked lamellae (Figure 8b). Good interfacial contact is evident by the absence of visible interlamella pores. Lamella orientation is closely parallel to the substrate, generating a thoroughly uniform coating with good structural integrity. The quality of the SHA coatings is considerably better than coatings deposited using agglomerated calcined HA and spray-dried HA powders. In fact, recent tensile-adhesion test results support this sensitive dependence of mechanical properties on microstructure. The bond strength of the densely packed SHA coatings measured according to ASTM 633 is significantly higher than the porous CHA coatings.

Phase composition of the plasma-sprayed SHA coating is generally a mixture of ACP and crystalline HA with traces of α-TCP and TTCP. Crystallinity is decreased because of complete melt-

ing and rapid solidification. Preferential formation of the various phases can be promoted through selective sizing of the powder feedstock.

Similar coating characteristics are observed when adopting other spray techniques such as HVOF. An additional feature in the HVOF coatings is the increased presence of respheroidized droplets on the surface. These are in the size range of 1–2 μm. The as-sprayed SHA coating surface generated by HVOF is similar to plasma-sprayed SHA coatings. Good melting of the particles is evident by the formation of disc-shaped splats. The splats are well intact without fragmentation, in spite of the high particle velocity. There is little evidence of granular areas reported in a recent study on HA coating deposited by HVOF using particle feed in the size range of 15–115 μm.[74] The SEM observation of the polished cross section revealed a dense coating with good interlamella contacts.

The investigation of plasma-sprayed HA coatings revealed significant effects relating particle morphology of the feedstock to the characteristics of the sprayed coatings. The characteristics of the starting material regarding size, structure, and composition can affect the final coating characteristics with respect to microstructure, phase composition, crystallinity, and surface morphology. Using agglomerated powders that are either angular (calcined and crushed HA) or spherical (spray-dried HA) tends to produce porous coating microstructures. This is mainly associated with deposition inconsistency caused by particle breakdown in the plasma flame. On the other hand, dense, spherical HA powders that are formed through combustion-flame spheroidization of the crushed HA yield lamella structures that are dense and coherent when plasma sprayed.[75] Also, the formation of certain phases through selective sizing of the powder feedstock is more attainable because of the stability of the dense particles.

Recent XRD data show that the flame-spheroidized HA powders undergo only negligible amorphization, unlike plasma-sprayed HA powders.[76,77] Having this relationship between phase formation and particle size permits the use of a narrow particle-size range to effect specific phase formation in the as-sprayed coatings. The physical characteristics of the starting material emanated from selective particle processing has significant effects on the final properties of the coating.

Tensile-bond strength tests were carried out on an Instron 4302 (10 kN load cell) universal tester in accordance to ASTM F 1501-94. The type of adhesive used for the tensile-adhesive test was a cold-cured 3M-DP460 epoxy adhesive comprising a duo-pak and applicator.

The tensile-adhesion tests (TATs) were performed with a cross head speed of 1 mm/min. TAT data of CHA on titanium are shown in Table II. TAT data for SHA coatings on titanium and stainless steel are shown in Table III. The average bond strength of CHA is around 22.6 MPa. The failure mode in these coatings is a combination of cohesive and adhesive failure. The adhesive strength of SHA averages around 8.7 MPa, while its cohesive strength is about 29.2 MPa. Variations in coating thickness had little effect on the cohesive bond strength. The fracture strength of the adhesive glue is 38.7 MPa.

Microstructural examination indicated that the coating integrity of SHA coatings is higher than CHA coatings. This improvement in coating quality is mainly due to the spherical geometry and surface and structural morphology of the SHA powder, which enhances flowability, particle stability, and deposition consistency. Knowing that the mechanical property is a sensitive function of microstructure, the cohesive strength of SHA was, therefore, expected to be higher. This was verified by TAT measurements; however, the strength differences were not very apparent, as predicted.

A probable explanation for this is the strengthening of the porous CHA coating by the penetration of the TAT glue. Energy-dispersive x-ray analysis (EDAX) of the fracture surface detected the presence of glue in the larger voids. This suggests that the overall bond strength is a combination of both coating and epoxy. Considering a coating thickness of around 159 μm, glue penetrating through the porous coating

Table III. Tensile Adhesion Test Data of Plasma-Sprayed SHA Coatings on Titanium and Stainless Steel

Test Number	Coating Thickness (μm)	Tensile Stress (MPa)	Fracture Mode
On Titanium			
TS1	300	35.94	Cohesive
TS2	310	26.54	Cohesive
TS3	400	34.70	Cohesive
TS4	320	23.62	Cohesive
TS5	280	29.39	Cohesive
TS6	400	25.20	Cohesive
Mean	335	29.23	
On Stainless Steel			
SS1	290	8.34	Adhesive
SS2	275	9.17	Adhesive
SS3	261	9.18	Adhesive
SS4	288	8.18	Adhesive
Mean	278.5	8.72	

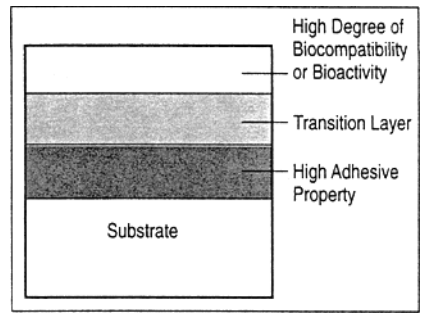

Figure 9. A schematic of the functions of the layers in a functionally graded coating.

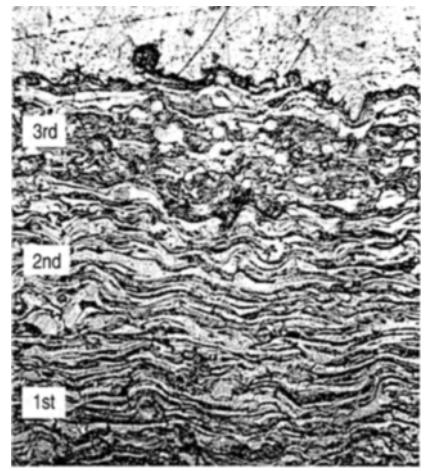

a

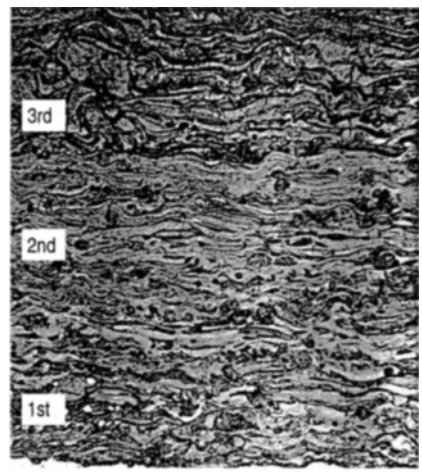

b

Figure 10. Cross sections of (a) SHA FGC (first layer [SHA]—20~45 μm; second layer—45~75 μm; third layer—75~125 μm) and (b) TCP/SHA FGC (first layer [SHA]—20~45 μm;second layer—TCP/HA; third layer—spherical α-TCP).

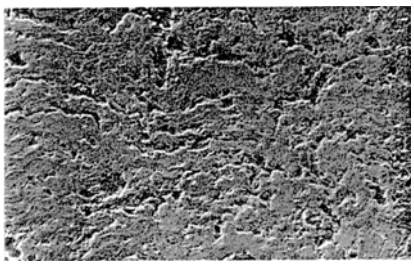

a 100 μm

b 100 μm

Figure 11 (a) The cross section of plasma-sprayed Ti-6Al-4V/HA coating with (b) evidence of pull-outs during polishing.

could not be ruled out. EDAX analysis did not detect the presence of epoxy in the dense SHA coating. Considering the coherent nature of the coating and the thickness of the coating (reaching 400 μm), the possibility of glue interference is less likely. Judging from the fracture behavior, the TAT bond strength is a good approximation of the cohesive strength of as-sprayed HA.

It is worthwhile to note that although a higher cohesive strength is achieved with denser coating, it is only beneficial if the adhesive strength is comparable. The limiting strength of a coating system is governed by the binding forces acting between substrate-lamella or lamella-lamella interfaces. The other drawback is the amorphous character in the as-sprayed coating. However, on-going investigations have indicated the benefits of hot isostatic pressing (HIPing) to not only improve interfacial properties (adhesive strength), but also to restore crystallinity and densification by closing interlamellar pores.

FUNCTIONALLY GRADED COATINGS BASED ON CALCIUM PHOSPHATES

Functionally graded materials (FGMs) have a gradient compositional change from the surface to the interior of the material. With the unique microstructure of an FGM, material for specific function and performance requirements can be designed. The potential value of FGMs has attracted much attention in different fields such as aerospace, electrical power generation, etc.[78,79] In the field of biomaterials, several approaches have been attempted to develop functionally graded biomaterials for implants.[80,81] This study attempted to develop functionally graded coatings (FGC) of various calcium phosphates by primarily utilizing two approaches: making use of the "natural" response of various particle-size ranges of HA powders in the plasma to generate a coating that combines a strong adhesive quality at the substrate end and good bioactive property at the top coat (explored with SHA powders) and developing a coating system that will have accelerated osseo-induction properties by having a plasma-sprayed, bioresorbable α-TCP top coat. The intermediate coat is composed of α-TCP and HA, while the bottom layer is HA.

Functionally graded calcium-phosphate coatings (Figure 9) were designed to probe the possibility of combining the advantages of different calcium-phosphate coatings to suit the various requirements at different stages of the foreign material in the human body. The SHA FGC system is graded by SHA with different particle sizes. Previous studies[75,76] revealed that the particle-size range and shape of HA feedstock will affect the microstructure and phase composition of coatings. The first layer of the SHA FGC coating on the titanium substrate is SHA ranging from 20 μm to 45 μm, which provides a dense coating structure that should result in a higher adhesive strength. The top layer is deposited by large particles of HA (75~125 μm) that can produce highly crystalline and porous HA coatings.

The α-TCP/HA system was designed to provide improved bioresorbability of the coating surface. The top layer is deposited with α-TCP, which could provide calcium and phosphate materials for accelerated bone formation. The first layer is the same as that of the SHA system, and the intermediate layer is a mixture of α-TCP and HA. Tricalcium phosphate [TCP, $Ca_3(PO_4)_2$], known in its two polymorphs of α-TCP and β-TCP, is a bioresorbable ceramic that dissolves gradually in body fluid as new bone eventually replaces it. The solubility of α-TCP is higher than β-TCP. Harada found that a mixture of α-TCP and HA bonds with bone faster than HA alone.[82] The main reason is that α-TCP dissolves around HA and provides calcium and phosphate, which are essential for bone to grow onto the surface of the implant. In vivo testing conducted by Claes et al. showed that the volume of newly formed bone on a TCP surface is higher than that on a HA surface.[83] The arrangement of the TCP/HA FGC has the propensity of allowing accelerated biointegration of the coating by the body tissues as the top layer gets rapidly resorbed, leaving the more biocompatible intermediate layer to facilitate the much-needed biocompatibility for proper osteoconduction.

A cross section of SHA FGC (Figure 10a) revealed a more porous microstructure, with more unmelted particles with larger SHA powders. The pores are relatively fewer, with smaller SHA powders. XRD patterns show that the crystallinity of HA and the amount of TCP, TTCP, and CaO phases vary as the particle size of SHA feedstock. It is easy for small particles to decompose when totally melted in high temperature. As for bigger particles, they would be only partially melted. The chemical decomposition and phase transformation is much less than that in totally melted droplets. The surface of the SHA FGC is mainly composed of crystalline HA, with small amounts of decompositional phases and amorphous phase, which implies a high biocompatibility.

The flame-spheroidization process was used to prepare the spherical α-TCP pow-

References

1. J.D. de Bruijn, C.A van Blitterswijk, and J.E. Davies, *J. Biomed. Mater. Res.*, 29 (1995), pp. 89–99.
2. M. Jarcho et al., *J. Bioeng.*, 1 (1977), pp. 79–92.
3. R.M. Pilliar, J.E. Davis, and D.C. Smith, *MRS Bull.*, 16 (9) (1991), pp. 55–61.
4. R.G.T. Geesink and N.H.M. Hoefnagels, *J. Bone and Joint Surgery*, 77-B (4) (1995), pp. 534–547.
5. K. Søbelle et al., *Acta Orthop. Scand*, 4 (1990), pp. 299–306.
6. S.D. Cook et al., *Clin. Orthop.*, 230 (1988), pp. 303–312.
7. S.Y. Chao and C.K. Poon, *J. Oral Max. Surg.*, 45 (1987) p. 359.
8. H. Denissen, C. Mangano, and G. Venini, *Hydroxyapatite Implants* (Padua: Piccin Nuova Libraria, S.P.A., 1985), p. 19.
9. S.M. Best and W. Bonfield, *J. Mater. Sci.: Mater. Med.*, 5 (1994), pp. 516–521.
10. G.L. de Lange et al., *J. Dent. Res.*, 68 (1989), p. 509.
11. S.D. Cook et al., *J. Biomed. Mater. Res.*, 26 (8) (1992), pp. 989–1001.
12. K. de Groot et al., *J. Biomed. Mater. Res.*, 21 (12) (1988), pp. 1375–1381.
13. P. Ducheyne et al., *J. Biomed. Mater. Res.*, 14 (1980), pp. 225–237.
14. R.G.T. Geesink, K. de Groot, and C.P.A.T. Klein, *J. Bone Joint Surg.*, 70B (1988), pp. 17–22.
15. B.C. Wang et al., *J. Mater. Sci.: Mater. Med.*, 4 (1993), p. 394.
16. P. Ducheyne and K. Healy, *J. Biomed. Mater. Res.*, 22 (12) (1988), pp. 1137–1163.
17. K.A. Thomas et al., *J. Arthroplasty*, 4 (1) (1989), pp. 45–53.
18. J.F. Kay, *Dent. Clin. of North America*, 36 (1) (1992), p. 1–18.
19. R.G.T. Geesink, *Clin. Orth. Rel. Res.*, 261 (1990), pp. 39–58.
20. H. Ji, C.B. Ponton, and P.M. Marquis, *J. Mater. Sci.: Mater. Med.*, 3 (1992), pp. 283–287.
21. T.W. Bauer et al., *J. Bone Joint Surg.*, 73-A (10) (1991), pp. 1439–1451.
22. P. Ducheyne et al., *Biomaterials*, 11 (1990), pp. 244–254.
23. H. Oguchi et al., *Biomaterials*, 13 (1992), pp. 471–477.
24. W. Van Raemdonck, P. Ducheyne, and D.P. Meester, *J. Am. Ceram. Soc.*, 67 (6) (1984), pp. 381–384.
25. M. Yoshinari, O. Yoshiro, and T. Dérand, *Biomaterials*, 15 (7) (1994), pp. 529–535.
26. J.G.C. Wolke et al., *J. of Bio. Mat. Res.*, 28 (1994), pp. 1477–1484.
27. K. Yamashita et al., *J. Am. Ceram. Soc.*, 77 (9) (1994), pp. 2401–2407.
28. C.M. Cotell et al., *J. Appl. Biomater.*, 3 (1992), p. 87.
29. C. Chai et al., *Mat. and Man. Proc.*, 10 (2) (1995), pp. 205–216.
30. G. Schwier and C. Hermann, *Proc. 11th ITSC* (Kobe, Japan: High Temp. Society Japan, 1986), pp. 277–282.
31. C.C. Berndt and K. A. Gross, *Proc. ITSC* (Kobe, Japan: High Temp. Society Japan, 1992), pp. 465–470.
32. F.J. Hermanek and A.R. Nicholl, *Proc. of 1st NTSC*, ed. D. Houck (Materials Park, OH: ASM, 1986), pp. 337–344.
33. D.M. Liu, H.M. Chou, and J.D. Wu, *J. Mater. Sci.: Mater. Med.*, 5 (1994), pp. 147–153.
34. P.E. Wang and T.K. Chaki, *J. Mater. Sci.: Mater. Med.*, 4 (1994), pp. 150–158.
35. S.R. Radin and P. Ducheyne, *J. Mater. Sci.: Mater. Med.*, 3 (1992), pp. 33–42.
36. B. Koch, J.G.C. Wolke, and K. de Groot, *J. Biomed. Mater. Res.*, 24 (1990), pp. 655–667.
37. H.H. Douglas, *Proc. 3rd NTSC* (Materials Park, OH: ASM, 1990), pp. 419–423.
38. S.R. Brown, I.G. Turner, and H. Reiter, *J. Mater. Sci.: Mater. Med.*, 5 (1994), pp. 756–759.
39. M. Weinlaender et al., *J. Mater. Sci.: Mater. Med.*, 3 (1992) pp. 397–401.
40. C.P.A.T. Klein et al., *J. Biomed. Mater. Res.*, 25 (1991), pp. 53–65.
41. W.R. Lacefield, *Ann. N.Y. Acad. Sci.*, 523 (1988) p. 72.
42. J.G.C. Wolke et al., *J. Thermal Spray Technol.*, 1 (1) 1992), pp. 75–82.
43. C.Y. Yang et al., *J. Mater. Sci.: Mater. Med.*, 6 (1995), pp. 249–257.
44. R. McPherson, N. Gane, and T.J. Bastow, *J. Mater. Sci.: Mater. Med.*, 6 (1995), pp. 327–334.
45. C. Doyle, *Handbook of Bioactive Ceramics*, 2, ed. T. Yamamuro, L.L. Hench, and J. Wilson (Boca Raton, FL: CRC Press, 1990), pp. 195–208.
46. W. Bonfield, *Bioceramics: Materials Characterisation vs In vivo Behaviour*, 523, ed. J. Lemon and P. Ducheyne (New York: New York Academy of Sciences, 1988) pp. 173–177.
47. P. Ducheyne and J.F. McGucken, Jr., *Handbook of Bioactive Ceramics, vol. II, Calcium Phosphate and Hydroxyapatite Ceramics*, ed. by T. Yamamuro, L.L. Hench, and J. Wilson (Boca Raton, FL: CRC Press, 1990) pp. 185–186

der. TCP/HA composite powder was produced by ball milling (ball milling parameter was 120 revolutions per minute for 60 minutes) and spray drying. Polyvinyl acetate (PVA) (1 wt.%) was used as a binder, and a debinding process was conducted at 400°C for two hours, followed by sintering at 800°C for two hours. A cross-section of the TCP/HA FGC (Figure 10b) is relatively dense and free of large pores. A lamellar structure without an obvious boundary between the layers can be observed. The XRD spectra of the as-sprayed TCP/HA FGC shows that the first layer is composed of HA, TCP, CaO, TTCP, and ACP, while crystallized TCP and ACP were the main phases in the top layer, suggesting a high bioresorbability.

PREPARING AND PLASMA SPRAYING HA-BASED COMPOSITES

Flame spraying was used to spheroidize the composite HA-ZrO_2 mixture.[84] Similar surface morphologies were observed with the spheroidized HA powders, which ranged from 2–40 μm. However, a cross section reveals a composite profile comprising small fragments of yttria partially stabilized zirconia encased within a HA-rich spherical particle. The XRD analysis of the powder showed the presence of tetragonal ZrO_2, HA, and α-TCP phases. This clearly demonstrates the ability of thermal spraying to produce composite powders with a dual-phase structure. The dense structure of the particle ensured particle stability during plasma spraying, and its spherical shape would improve flowability during its transport from the powder feeder to the plasma gun. The plasma-sprayed HA-ZrO_2 coatings contain similar phases to the flame-spheroidized powders. The ZrO_2 particles were present as fine dispersions, angular particles, and well-melted lamellae. The presence of angular particles indicates that there are some particles that are not melted sufficiently in the plasma.

The surface of the plasma-sprayed Ti-6Al-4V/HA composite coating is characterized by undulated structures and smooth splats that arose from a combination of partially melted and fully melted particles.[85] Some amounts of cracking are detected on the splats. These are likely due to residual stresses upon rapid solidification. Examination of the polished cross section revealed a typical lamellae structure consisting of alternating layers of Ti-6Al-4V and HA (Figure 11a). High-magnification observation shows that the HA-rich regions are mechanically weak, and evidence of pull-outs during polishing can be observed rather vividly (Figure 11b). In addition, some HA-rich lamella have cracks. These cracks need to be "healed" in order for the composite coatings to have reasonable mechanical strength during usage.

CONCLUSION

The flexibility of thermal spraying provides numerous options and possibilities to counter difficulties or demands presented by specific applications. In biomedical applications where coating requirements are many and often difficult to achieve in a single process step, this variability has certain apparent advantages. Some of these requirements could be met by using correctly sized powders to generate dense coatings rich in certain phases, applying high-kinetic spray systems to effect better coating formation without excessive melting to surcease certain undesirable high-temperature phases, forming a graded coating by selective deposition, spraying with a composite material with phase constituents that are complimentary to each other, and using a post-spray treatment to enhance the coating characteristics.

The study reported here has demonstrated the dual function of thermal spraying to perform powder processing such as spheroidization and coating deposition of bioceramics. Thermal-spray spheroidization opens up a new concept for powder processing that can result in pure HA with suitable physical properties (e.g., flowability) that are needed for optimized plasma spraying. These spheroidized powders are highly dense with good structural stability and do not break down to create further complications during plasma spraying. The spherical geometry also ensures deposition consistency through optimized heating of the particles in the plasma or HVOF flames.

The use of small SHA powders is found suitable for novel thermal-spray techniques such as HVOF. SEM observations of the sprayed coating reveal the coating to possess good melting and deposition characteristics. The HA-based composites have the potential of widening the application of HA by enhancing the mechanical properties. The combination of combustion-flame spray and plasma spray has enabled the production of HA-based composites with unique microstructures. Post-spray treatment with lasers or hot isostatic pressing may help to enhance the surface structure and mechanical properties of the coatings.[86,87]

ACKNOWLEDGEMENT

Financial support under Applied Research Grant Nos. RP 39/89 and RP 56/92 (Nanyang Technological University) is gratefully acknowledged.

48. A. Bishop et al., *J. Materials Science Lett.*, 12 (1993), pp. 1516–1518.
49. S. Oki et al., *Proc. of 13th International Thermal Spray Conference*, ed. C.C Berndt (Materials Park, OH: ASM, 1992), pp. 447–451.
50. C.S. Yip et al., paper submitted to *J. Mater. Proc. Technol.*
51. L.L. Hench, *J. Amer. Ceram. Soc.*, 74 (1991), pp. 1487–1510.
52. R.H. Doremus, *J. of Mat. Sci.*, 27 (1992), pp. 285–29.
53. I. Dion et al., *J. Mater. Sci.: Mater. Med.*, 5 (1994), pp. 18–24.
54. R.C. Garvie, R.H.J. Hannink, and N.A. McKinnon (1981), U.S. patent 4,279,655.
55. E.P. Butler, *Mater. Sci. Tech.*,1 (6) (1985), pp. 417–432.
56. A.G. Evans, *Adv. in Ceramics*, 12, ed. N. Claussen, M. Ruhle, and A.H. Heur (Westerville, OH: ACerS, 1984), pp. 193–212.
57. G.A. Gogotsi and M.V. Swain, *Science and Technology of Zirconia V*, ed. S.P. Badwal, M.J. Bannister, and R.H.J. Hannink (New Jersey: Technomic Publishers, 1993), pp. 347–359.
58. M. Shimbo and M. Itoh, *Adv. in Ceramics* , 24A, ed. S. Somiya, N. Yamamoto and H. Yanagida (Westerville, OH: American Ceram. Soc., 1988),pp. 415–422.
59. N. Claussen, *J. Amer. Ceram. Soc.*, 59 (1-2) (1976), pp. 49–51; N. Claussen and J. Jahn, *J. Amer. Ceram. Soc.*, 63 (3–4) (1980), pp. 228–229.
60. P. Christel et al., *J. Biomed. Mat. Res.*, 23 (1989), pp. 45–61.
61. R.C. Garvie et al., *J. Mater. Sci.*, 19 (1984), pp. 3224–3228.
62. J.H. Chern Lin, M.L. Liu, and C.P.O. Ju, *J. Mater. Sci.: Mater. Med.*, 5 (1994), pp. 279–283.
63. J. Li, S. Forberg, and L. Hermansson, *Biomaterials*, 12 (1991), pp. 438–440.
64. H. Ji and P.M. Marquis, *Biomaterials*, 13 (11) (1992), pp. 744–748.
65. J.D. Santos et al., *Biomaterials*, 15 (1994), pp. 5–10.
66. B. Fartash et al., *J. Mater. Sci.: Mater. Med.*, 6 (1994), pp. 451–454.
67. K. Ioku, M. Yoshimura, and S. Somiya, *Biomaterials*, 11 (1990), pp 57–61.
68. M. Takagi et al., *J. Mater. Sci.: Mater. Med.*, 3 (1994), pp. 199–203.
69. S. Somiya et al., *Ceramic Powder Science and Technology, Advances in Ceramics*, 21 (Westerville, Ohio: ACerS, 1987), pp. 43–53.
70. K.A. Khor and P. Cheang, *Thermal Spraying Conference NTSC '94*, ed. CC. Berndt and S. Sampath (Materials Park, OH: ASM, 1994), pp. 147–152.
71. P. Cheang and K.A. Khor, *J. Mater. Proc. Technol.*, 48 (1995), pp. 429–436.
72. K.A. Khor and P. Cheang, *J. Thermal Spray Technol.*, 3 (1) (1994), pp. 45–50.
73. K. de Groot, *J. Ceram. Soc. Japan*, 99 (1991), pp. 943–953.
74. J.D. Haman, L.C. Lucas, and D. Crawmer, *Biomaterials*, 16 (3) (1995), pp. 229–237.
75. P. Cheang and K.A. Khor, *J. of Therm. Spray Tech.*, 5 (3) (1996), pp. 310–316.
76. P. Cheang and K.A. Khor, *Biomaterials*, 17 (1996) pp. 537–544.
77. K.A. Khor and P. Cheang, unpublished results (1996).
78. M. Koizumi and M. Niino, *MRS Bulletin* (Jan., 1995), pp. 19–21.
79. S.W. Huelsman and W.G.J. Bunk, *Advanced Materials'93*, vol. 16B, ed. M. Sakai et al. (Japan: Tran. Mat. Res. Soc., 1994), pp. 1259–1262
80. M. Kon et al., *Biomaterials*, 16 (1995), pp. 709–714.
81. J.A. Kerdic, A.J. Ruys, and C.C. Sorrell, *Int. Ceram. Monogr.* 1 (1) (1994), pp. 215–221.
82. Y. Harada, *J. of Tokyo Dent. College Soc.* (1989), pp. 263–297.
83. L. Claes et al., *Handbook of Bioactive Ceramics, Vol II, Calcium Phosphate and Hydroxyapatite Ceramics*, ed. T. Yamamuro, L.L. Hench, and June Wilson (Boca Raton, FL: CRC Press, 1990), pp. 77–86.
84. K.A. Khor, C.S. Yip, and P. Cheang, *8th Int. Conf. on Biomedical Engrg.*, ed. J.C.H. Goh and A. Nather (Singapore, 1994), pp. 536–538.
85. K.A. Khor and P. Cheang, *J. Thermal Spray Tech.*, in press.
86. K.A. Khor, C.S. Yip, and P. Cheang, *J. Mater. Proc. Technol.*, in press.
87. P. Cheang et al., *Biomaterials*, 17 (19) (1996) pp. 1901–1904.

ABOUT THE AUTHORS

K.A. Khor earned his Ph.D. from Monash University in 1989. He is currently a senior lecturer at the School of Mechanical and Production Engineering at Nanyang Technological University (NTU) in Singapore.

P. Cheang earned his Ph.D. from Monash University in 1990. He is currently a senior lecturer at the School of Applied Science at NTU in Singapore.

Y. Wang earned her B.Eng. degree from Beijing University of Aeronautics and Astronautics in China in 1989. She is currently pursuing her M.Eng. at the School of Mechanical and Production Engineering at NTU in Singapore.

For more information, contact K.A. Khor, School of Mechanical and Production Engineering, Nanyang Technological University, Nanyang Avenue, Singapore 639 798; telephone 011-65-791-1744, ext. 5526; fax 011-65-791-1859; e-mail mkakhor@ntuvax.ntu.ac.sg